

Multi-wavelength observation of MAXI J1348–630 during the recent outburst using ALMA/Chandra/NuSTAR

Debasish Saha

Midnapore City College, Kuturia, Bhadutala, West Bengal, India 721129

Sabyasachi Pal

Indian Centre for Space Physics, 43 Chalantika, Garia Station Road, Kolkata, India 700084

Midnapore City College, Kuturia, Bhadutala, West Bengal, India 721129

Manoj Mandal

Midnapore City College, Kuturia, Bhadutala, West Bengal, India 721129

and

Arijit Manna

Midnapore City College, Kuturia, Bhadutala, West Bengal, India 721129

ABSTRACT

We studied the multi-wavelength timing and spectral properties of the high mass X-ray binary MAXI J1348–630 during two successive outbursts of April and June 2019 (from MJD 58596 to MJD 58710) using ALMA, Swift, Chandra and NuSTAR. We studied the first broadband spectrum for this black hole that includes fluxes in radio, optical, ultraviolet and X-ray energy bands. We have used the high-resolution ALMA data to study the millimetre radio emission from compact jets in band 3, 4, 6 and 7 (89.56–351.44 GHz). The ultraviolet and X-ray counterparts are found using UVOT ($\lambda = 2246 \text{ \AA}$) and XRT (0.9–9 keV) onboard the Swift observatory. The X-ray spectrum is intensively studied using NuSTAR data in the range of 3–70 keV. We have studied the interday variation of spectral parameters of the source using three NuSTAR observations (from MJD 58655 to MJD 58672) during the hard state of the outburst of June. We have detected low-frequency quasi-periodic oscillation using NICER data on MJD 58654 with a significance of 6.8σ at frequency 0.82 Hz in the hard state with RMS variability of 7.6 per cent. Another QPO has been detected at 0.67 Hz on MJD 58655 using NuSTAR data with a significance of 5.58σ and 2.1 per cent RMS. The hardness ratio shows significant variation during the outburst of April but remained almost

constant during the outburst of June. The spectral evolution in the hardness intensity diagram is studied during the outbursts. The position of the source is measured by Chandra that gives RA=13h48m12.878s, Dec=−63°16'28.85" with enhanced accuracy.

Subject headings: accretion, accretion disks – black hole physics – X-rays: binaries – X-ray: individual (MAXI J1348–630)

1. Introduction

Blackhole transients are known to accrete matters from their companion stars in the form of an accretion disk which often results in outburst. Matters are supplied to the black hole in the form of disk winds and jets are generated. The transition between different states and variation of timing and spectral properties are generally observed during the time of outburst (Homan & Belloni 2005).

A black hole evolves through various spectral states (Remillard & McClintock 2006; Belloni 2009) during an outburst. It evolves as Hard State (HS) → Hard-intermediate State (HIMS) → Soft-intermediate State (SIMS) → Soft State (SS) (Homan & Belloni 2005) during the rising phase of outburst. On the decaying phase of the outburst, the source returns to the HS following the reverse order (Motta et al. 2011; Homan & Belloni 2005; Belloni, Motta & Muñoz-Darias 2011; van der Klis 2006). These states can be well observed by studying the hardness-intensity diagram (HID) (Homan et al. 2001), hardness-RMS diagram (HRD) (Belloni et al. 2005), RMS-intensity diagram (RID) (Muñoz-Darias, Motta & Belloni 2011) etc. During an outburst, most of the sources evolve through these states following the above-mentioned order creating a ‘q’ shaped track in HID (Homan & Belloni 2005; Dunn et al. 2010). But all black holes do not necessarily follow this order. There are some sources also that does not show any state transition during the entire outburst and are known as “failed outburst” (Sturner & Shrader 2005; Capitanio et al. 2009; Del Santo et al. 2016).

During SS, accretion disks are relatively hotter with a typical disk temperature of $kT \approx 1$ keV (Dunn et al. 2010) and thermal X-rays are emitted from the innermost part of the accretion disk. In HS the accretion disks become relatively cooler (Miller et al. 2008). Multi-wavelength observations help to understand emission mechanisms from different regions of the source, accretion phenomenon or transition through different states during the outburst of a black hole X-ray Binary (BHXRb).

Black hole binaries are known to emit strong radio emission from the compact jet in the HS (Fender 2006) and a correlation between radio and X-ray luminosities are found

to be present which indicates a coupling nature between the jets and the accretion disk (Corbel et al. 2003).

The BHXR transient MAXI J1348–630 was discovered during a giant outburst in January 2019 (Yatake et al. (2019); we will mention it as the first outburst). Two subsequent outbursts continued in April 2019 (regarded as the second outburst) and June 2019 (Negoro et al. (2019); regarded as the third outburst). During the first outburst, the averaged flux reached a maximum of ~ 4 Crab as measured by MAXI/GSC in the energy range 2–20 keV (Tominaga et al. 2020). The second outburst of relatively smaller magnitude started in the last week of April 2019 before the outburst of January completed its decaying phase (Negoro et al. 2019). Previous observations suggest that the source is a black hole candidate (Sanna et al. 2019; Tominaga et al. 2020; Zhang et al. 2020). Jana et al. (2020) estimated the mass of the black hole to be $\sim 9M_{\odot}$ and the source distance is approximately 5–10 kpc. From the first outburst, two low-frequency QPOs – at frequency 0.57 Hz and 0.66 Hz (Jana et al. 2020) and several type-B QPOs between 4.514 Hz and 4.096 Hz are detected (Belloni et al. 2020).

In this paper, we have studied the evolution of different timing and spectral properties of the black hole MAXI J1348–630 during the outburst of April and June 2019. Observation and data analysis methods of different instruments are discussed in section 2, results are summarised in section 3. Discussions are made in the section 4 and the results have been concluded in section 5.

2. Observations and data analysis

2.1. ALMA

We have used the high-resolution Atacama Large Millimeter/Submillimeter Array (ALMA)¹ interferometric 12 m array data for exploring the radio properties of black hole MAXI J1348–630. The observation was done on 02 May 2019 starting from 03h07m29.7s UTC. The observational summary is given in Table 1. During the observation, the device was set up in band 3, 4, 6, and 7 with four spectral windows. The bandwidth of all science spectral windows is 187.50 MHz which is divided into 1920 channels. The black hole was observed in ALMA band 3 to band 7 with XX, YY signal substances via integration time 1149.120 s. During the observation, a total of 43 antennas was working with a baseline ranging from 42 to 1574 m respectively. The antenna temperature did not exceed above 100 K because the environmen-

¹<https://www.almaobservatory.org/en/home/>

tal condition was very good. During the observation, the source J1427–4206 was observed as a bandpass, and flux calibrator but J1337–6503 was observed as a phase calibrator. We have used Perley-Butler 2017 for flux scale calibration (Perley & Butler 2017).

We have used the Common Astronomy Software Application (CASA v 5.4.1)² for initial data reduction and continuum imaging of black hole MAXI J1348–630 with standard calibration scripts. After calibration, we have used the task **MSTRANSFORM** to split the corrected target data set and making the continuum image of the source using task **TCLEAN** operation with the stokes I parameter. The image is deconvolved several times with 12000 iterations. We have also used the task **UVCONTSUB** for background noise subtraction and several selfcal processes. The self-calibration process is done by the tasks **GAINCAL** and **APPLYCAL**.

2.2. Chandra

The Chandra observatory uses mirrors with multiple instruments to focus and collect X-rays from highly energetic celestial objects. The focal plane consists of two science instruments – Advanced CCD Imaging Spectrometer (ACIS) and High-Resolution Camera (HRC) which captures the high-resolution images created by the mirrors and collects information about incoming X-rays. There are two other science instruments onboard Chandra for high-resolution spectroscopy – the High Energy Transmission Grating (HETG) (Canizares et al. 2005) and Low Energy Transmission Grating (LETG) (Brinkman et al. 2000) spectrometers. ACIS and HRC measure the position of the source to determine the energy appropriately. Science instruments on board Chandra have the capabilities to collect and analyze X-ray images and properties of celestial bodies with exceptional accuracy having an angular resolution of 0.5'' over the energy range of 0.2–10 keV.

The Chandra observation of the black hole binary MAXI J1348–630 was made using the Advanced CCD Imaging Spectrometer (ACIS) array during the outburst with HETG (Obs Id – 21239, 21240, 21241). The observation log is shown in Table 1. We have analysed these data using CIAO v 4.12 with the latest CALDB v 4.9.4. We followed the standard Chandra data analysis threads for data reduction and analysis.

²<https://casa.nrao.edu/>

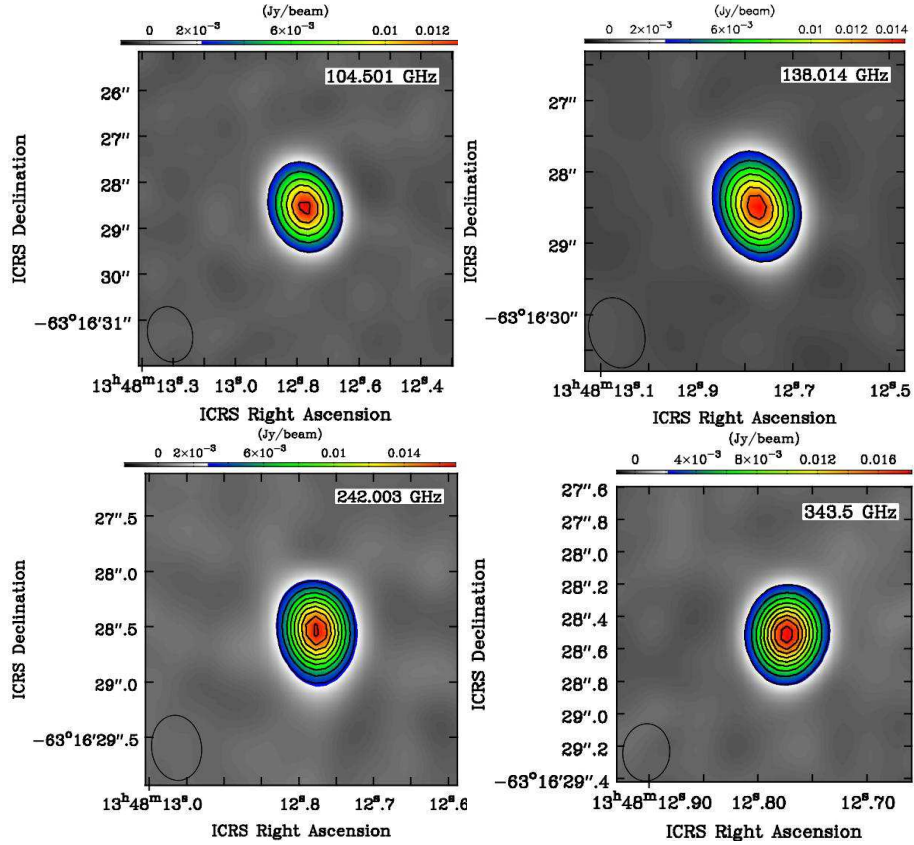


Fig. 1.— ALMA continuum image of black hole MAXI J1348–630 obtained on 2019 May 2 at 104.501 GHz, 138.014 GHz, 242.003 GHz and 343.500 GHz frequencies and computed using natural weight. The synthesized beam for observations with each frequency are shown in one corner of each images. The relative contour levels are 2, 4, 6, 8, 10, 12, 14, 16, 18 mJy.

Table 1: Log of ALMA, Chandra, NuSTAR, NICER and Swift observations

Instrument	Observation Id	Band	Date	Start Time	MJD	Exposure (ks)
ALMA	2018.1.01034.T	Band-3 (89.56–105.43 GHz)	2019-05-02	04:15:00	58605.18	1.104
ALMA	2018.1.01034.T	Band-4 (137.06–152.93 GHz)	2019-05-02	04:34:00	58605.19	1.150
ALMA	2018.1.01034.T	Band-6 (223.07–105.43 GHz)	2019-05-02	03:50:00	58605.16	1.279
ALMA	2018.1.01034.T	Band-7 (335.56–351.44 GHz)	2019-05-02	03:06:00	58605.13	2.670
Chandra	21239	—	2019-06-21	10:59:15	58655.45	19.120
Chandra	21240	—	2019-06-26	16:12:33	58660.67	20.120
Chandra	21241	—	2019-07-07	11:03:44	58671.46	20.130
NuSTAR	80502304002	—	2019-06-21	09:21:09	58655.38	13.784
NuSTAR	80502304004	—	2019-06-26	11:46:09	58660.49	15.368
NuSTAR	80502304006	—	2019-07-08	08:46:09	58672.36	17.183
NICER	2200530160	—	2019-06-20	11:37:57	58654.48	2.162
Swift	00011107032	—	2019-05-03	09:25:35	58606.39	0.534 (XRT) 0.526 (UVOT)

2.3. NuSTAR

The Nuclear spectroscopic telescope array (NuSTAR) is a space-based X-ray satellite that operates in the energy range of 3–79 keV. It has two detector units – FPMA and FPMB (Focal Plane Modules – A and B) each located at the focus of two co-aligned optics units. Each detector unit is comprised of four segments made of Cadmium Zinc Telluride (CdZnTe or CZT) having a rectangular shape of dimension $20\text{mm} \times 20\text{mm} \times 2\text{mm}$, gridded into 32×32 pixels. Each detector has angular resolutions of $58''$ Half Power Diameter (HPD) and $18''$ Full-width at Half-Maximum (FWHM). Energy resolution of each telescope is 0.4 keV at 6 keV and 0.9 keV at 60 keV respectively with $13' \times 13'$ field of view ([Harrison et al. 2013](#)).

NuSTAR performed three observations towards MAXI J1348–630 during the HS of the outburst for 13.8 ks, 15.4 ks and 17.2 ks exposure time (Obs Ids – 80502304002, 80502304004 and 80502304006 respectively). Summary of the data products is given in Table 1. NUPipeline tool is used to produce the level 2 data from which we have extracted light curves, images and spectra using the tool NUPRODUCTS provided by NUSTARDAS package. Data processing has been done using HEASOFT v 6.25 software with the recent version of the calibration database.

Interday variation of the spectral parameters of the source during the decaying phase of the outburst has been studied using NuSTAR data. Spectra are plotted using XSPEC v 12.10.1 ([Arnaud 1996](#)) with necessary Response Matrix Files (RMFs) and Ancillary Response Files (ARFs) that were produced by running NUPRODUCTS. Spectra are plotted in the energy range 3–70 keV, because outside this range photon statistics are not very significant. We have tried different models to fit the spectra that are discussed in the result section. Variation of spectral parameters are given in Table 2.

2.4. NICER

The Neutron star Interior Composition Explorer (NICER) on the International Space Station (ISS) is dedicated mainly to study neutron stars. The primary instrument of NICER is the X-ray Timing Instrument (XTI) which is an array of 56 X-ray photon detectors that collect photons in the energy range 0.2–12 keV ([Gendreau et al 2016](#)). After the discovery of MAXI J1348–630, NICER performed multiple observations towards the source. We have used the observation of 20 June 2019 (Obs Id – 2200530160) for the study of power spectral properties. We performed NICERL2 to apply the standard NICER calibrations and standard screening. We have applied barycenter correction by performing BARYCORR using ICRS as the reference frame. Light curves have been extracted using the barycenter corrected event

file in `XSELECT v 2.4e` with different bin sizes of 1 sec, 0.1 sec, 0.01 sec etc.

2.5. Swift

The Neil Gehrels Swift Observatory is a multi-wavelength observatory that operates in a wide range of energies including optical, ultraviolet, X-ray and gamma-ray wavebands by three different instruments onboard it. The Burst Alert Telescope (BAT) operates in the energy range of 15–150 keV which detects any event and the corresponding location in the sky (Barthelmy et al. 2005). BAT use to monitor the whole sky regularly. We have used daily monitoring data of Swift/BAT (15–50 keV) to plot the light curve (Figure 2) and HID (Figure 8).

The X-ray Telescope (XRT) onboard Swift operates in the energy range 0.3–10 keV to study the spectral properties of the source (Burrows et al. 2000). Since the resolution of XRT is better than that of BAT, it is often used to determine the location of any source with higher accuracy. XRT onboard Swift carried out observation for 0.534 ks on MJD 58606 in WT mode. We performed `XRTPIPELINE` using the level 1 event files and image files from the archived data to produce re-calibrated cleaned level 2 data products. We selected a source region and a background region using the imaging tool DS9. Using these calibrated, screened event files and regions files, we extracted high-level products (i.e. light curves, spectra and image files) from the task `XRTPRODUCTS`. The XRT spectrum is included in the broadband spectrum of Figure 4 in the energy range 0.9–9 keV.

Ultraviolet/Optical Telescope (UVOT) operates in both UV and visible regions with six different filters in it (1928–5468 Å) (Poole et al. 2008). UVOT observed the source for 0.526 ks in *uvw2* mode (central wavelength $\lambda = 2246 \text{ \AA}$) on MJD 58606. We checked if the UVOT image files are aspect corrected or not using the task `FKEYPRINT`. Since the correction was previously performed, we run `UVOTDETECT` for the source location on the UVOT sky image. We choose the source region as a circle of radius $10''$ around the source and the background region as an annulus with an inner and outer radius of $20''$ and $30''$ respectively keeping the source at the centre. We performed the routine `UVOTSOURCE` to examine the photometry of the source keeping the background threshold 5σ . The result has been used in the broadband spectrum in Figure 4.

We have extracted light curves using data of Swift/BAT (15–50 keV) and MAXI/GSC (2–20 keV). To study the hardness evolution, we have used MAXI/GSC data in the energy ranges 2–6 keV and 6–20 keV. We have used `FPLT` task in `FTOOLS`. We have also studied the power spectral properties of the source using the tool `POWSPEC` over different phases of

the outburst. To find the presence of QPOs, we have analysed Swift, NuSTAR and NICER data for different observations over the outburst. Power Density Spectrum (PDS) has been plotted using the task `POWSPEC` for different time bin sizes like 10 sec, 1 sec, 0.1 sec and 0.01 sec. We have used `LCMATH` tool for the background correction. The hardness intensity diagram has been plotted using MAXI/GSC hardness (6–20 keV/2–6 keV) and Swift/BAT flux (15–50 keV).

3. Results

3.1. Chandra and NuSTAR localization

On 26 January 2019, the new X-ray transient MAXI J1348–630 was discovered by MAXI/GSC and the measured position of the source was RA=13h48m12s, Dec=−63°04'04" (J2000) with 90 per cent C.L. elliptical error region having semi-major and semi-minor axes of 0.42° and 0.34° respectively (Yatake et al. 2019). Later, Denisenko et al. (2019) found the optical counterpart of MAXI J1348–630 using the iTelescope.Net T31 instrument and determined the position of the source as RA=13h48m12.88s, Dec=−63°16'28.4" (J2000). Using a 1 ks Target of Opportunity (ToO) observation with Swift, Kennea & Negoro (2019) found a bright source located at RA=13h48m12.73s, Dec=−63°16'26.8" (J2000) with 1.7" error radius (90 per cent confidence).

Chandra observed the black hole MAXI J1348–630 on 21 June 2019 with 19 ks exposure. Analysis of Chandra data reveals a bright point source located at RA=13h48m12.878s, Dec=−63°16'28.85" (J2000) with an error circle of 0.6". We also measure the position of the source using NuSTAR data of 21 June 2019. The position of the source measured by NuSTAR/FPMA is RA=13h48m13.065s, Dec=−63°16'24.03" (J2000). The position of the source measured by Chandra is about 2.16" away from the position measured by Swift/XRT and about 5.04" away from the position measured by NuSTAR. The optical counterpart of the source lies only 0.36" away from the Chandra measured position.

3.2. Temporal variations of X-ray emission

The Burst Alert Telescope (BAT) on board Swift³ and Gas Slit Camera (GSC) onboard MAXI⁴ are continuously monitoring the source from its discovery. In this study, we have focused on two subsequent outbursts that occurred between MJD 58596 and MJD 58709, covering 113 days approximately. Light curves using daily monitoring data of Swift/BAT and MAXI/GSC is shown in Figure 2. Variation of flux from the source observed by MAXI/GSC in 2–20 keV is shown in the upper panel (in red) and that using Swift/BAT in 15–50 keV is shown in the lower panel (in blue).

The second outburst of relatively smaller magnitude (compared to the first outburst) started at the end of April 2019 (MJD 58596) before the decaying phase of the first giant outburst reached its quiescent level and continued for almost 17 days. The flux reached the peak value 0.32 ± 0.01 Crab on MJD 58604 as measured by Swift/BAT (15–50 keV) and the peak flux measured by MAXI/GSC (2–20 keV) was 0.211 ± 0.005 Crab on MJD 58601.5. The outburst observed in 15–50 keV by Swift/BAT is comparatively more prominent than that observed in 2–20 keV by MAXI/GSC.

The next outburst with a comparatively larger magnitude was started in June 2019 (MJD 58630 approx) as observed by Swift/BAT. The outburst continued for almost 70 days and during the outburst, the flux reached a peak value of 0.83 ± 0.03 Crab on MJD 58653 as observed by Swift/BAT in the energy range 15–50 keV. The peak flux measured by MAXI/GSC in 2–20 keV is 0.301 ± 0.005 Crab on MJD 58654.5. The outburst was prominent with measurements by both MAXI/GSC in the energy range 2–20 keV and Swift/BAT in the energy range of 15–50 keV.

The source shows the variability of different time scales. Many micro-flaring activities are detected. In Figure 3, we have shown an example of a micro-flare of ~ 15 s duration that has been detected using NuSTAR data (Obs Id – 80502304002) on MJD 58655. The source shows a sharp rise and relatively slow decay, which is the typical nature of a micro-flare. It took ~ 5 sec to reach from 212 count s^{-1} to 486 count s^{-1} and ~ 10 s to come back in the base value.

³<https://swift.gsfc.nasa.gov/results/transients/>

⁴<http://maxi.riken.jp/top/index.html>

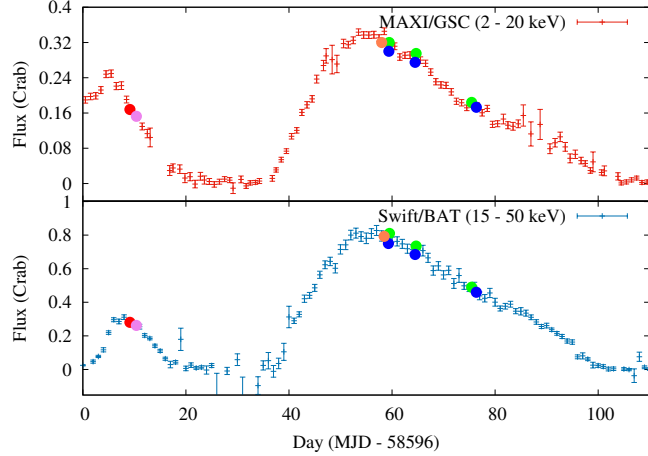


Fig. 2.— Variation of flux towards the source MAXI J1348–630 has been plotted during the outbursts of April and June 2019 using Swift/BAT and MAXI/GSC. In the upper panel, the variation of the flux using MAXI/GSC (in red) in the energy range 2–20 keV has been plotted while in the lower panel the variation of the flux as measured by Swift/BAT (in blue) in the energy range 15–50 keV is plotted. The nature of the variation of flux during the two successive outbursts in different energy ranges is observed. Each circle in the plot indicated the time of observations of different instruments over different phases of the outburst. Red and violet circles denote ALMA and Swift observations respectively, while orange, green and blue circles are to indicate NICER, Chandra and NuSTAR observations respectively.

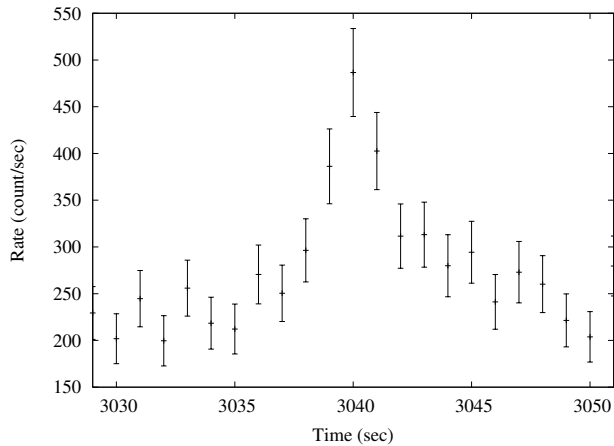


Fig. 3.— Several micro-flares are detected during the course of two outbursts. The figure shows example of a micro-flare of ~ 15 s that has been detected using NuSTAR data on MJD 58655 (Obs Id – 80502304002).

3.3. Broadband spectrum

The multi-wavelength spectrum is studied in a wide range of energy from radio to X-ray including ultraviolet and optical wavebands during the outburst of April. In Figure 4, we have shown the broad-band spectrum of the source using close-simultaneous observations. All observations were made between 2 and 3 May of 2019 when the source was close to the peak of the outburst of April. The ALMA observation was started at 03:06 UT on 2 May 2019 (MJD 58605.13) from which the radio emission from the compact jets is studied using different wavebands (band 3, 4, 6 and 7) with frequencies ranging from 89.56 GHz to 351.44 GHz. The Swift observation was performed at 09:25 UT on 3 May 2019 (MJD 58606.39). The ultraviolet observation was done by UVOT with *uvw2* filter having central wavelength $\lambda = 2246 \text{ \AA}$ onboard Swift observatory. The X-ray flux in 0.9–9 keV is included using data of XRT onboard Swift. We have also included the optical photometry from Gaia DR2 catalogue (Brown et al. 2018) in the plot for comparison.

The broadband spectrum is studied when the source was in the intermediate state, making a transition from SS to HS, near the peak of the April 2019 outburst during the decay phase. The source is strong in X-ray indicating weak emission from the jet.

3.4. Evolution of spectral parameters

Spectra of the source MAXI J1348–630 is plotted using NuSTAR/FPMA data. The spectrum has been plotted in the energy range 3–70 keV since outside this range the photon counts are not very significant. We studied the interday variation of the spectral parameters during the outburst. We have tried to fit all the spectra on different observations during the HS. The spectra are fitted with an absorbed broken power law. We added a blackbody component to take into account the blackbody emission from the accretion disk. The fit statistics enhanced significantly on adding a Gaussian component. The best-fitted parameters and their variation over the outburst are shown in Table 2. Figure 5 shows the spectrum and the residuals of the source using NuSTAR/FPMA data (Obs Id – 80502304004) that gives reduced $\chi^2 = 1.256$ for 1665 degrees of freedom.

Since the value of n_H is previously determined by Tominaga et al. (2020), we froze the value at $0.86 \times 10^{22} \text{ cm}^{-2}$ and set the other parameters free to vary. We obtained that the disk temperature is varying between 0.45 keV to 0.51 keV which is significantly lower compared to other black holes. Fluxes are obtained from the best-fitted model. Since the observations were made on the decaying phase of the outburst of June, the flux is gradually decreasing as observed in Table 2.

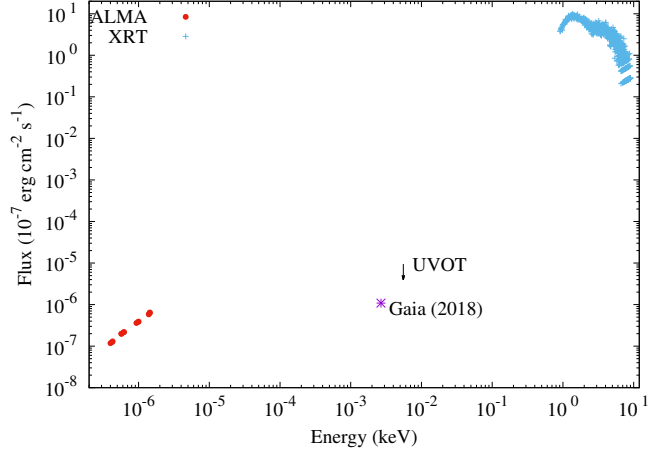


Fig. 4.— Broadband spectrum of the source MAXI J1348–630 from radio to X-ray band. The millimetre radio flux has been taken by analysing ALMA data which is shown by red circles. Ultraviolet and X-ray fluxes are included from UVOT and XRT data onboard the Swift observatory. The upper limit of the ultraviolet flux is denoted by a down arrow. The X-ray flux is shown by the blue points at the top right corner. The optical photometry has been taken from the Gaia DR2 catalogue, indicated by violet asterisk (Brown et al. 2018).

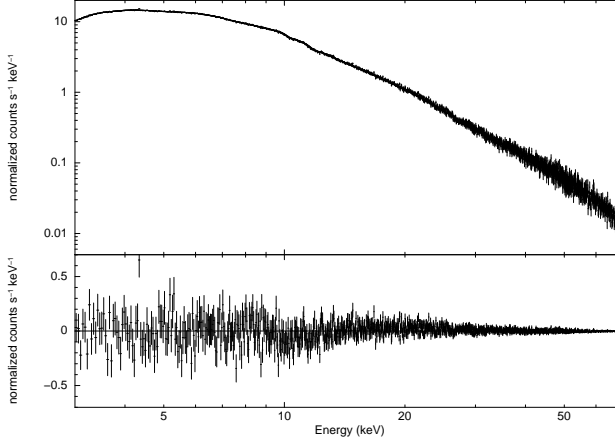


Fig. 5.— The spectrum of the source is plotted in the energy range 3–70 keV using NuSTAR/FPMA data (Obs Id – 80502304004) and has been well fitted with a combined model of $\text{phabs} \times (\text{bknpower} + \text{bbody} + \text{gaussian})$ with reduced $\chi^2 = 1.256$ for 1665 degrees of freedom.

3.5. Continuum Image of MAXI J1348–630 using ALMA

We detected the continuum emission from black hole MAXI J1348–630 between the frequency range of 89.56–351.44 GHz with ALMA band 3, 4, 6, and 7 observations. The continuum images of MAXI J1348–630 are shown in Figure 1. The source is not resolved in any of these frequencies.

The radio continuum spectrum of black hole MAXI J1348–630 is shown in Figure 6. The continuum radio spectrum shows the flat nature with spectral index (α) = -0.324 ± 0.003 (assuming $F_\nu \propto \nu^{-\alpha}$). The continuum image of black hole MAXI J1348–630 is shown the point source characteristics in ALMA observation bands. The ALMA measurements are included in the broadband spectrum of Figure 4. The slope of the spectrum is positive in the radio region, indicating that the synchrotron radiation is in an optically thick regime and the self-absorption frequency is more than 351.4 GHz.

3.6. Hardness evolution

The Hardness Ratio (HR) of the source during two successive outbursts is shown in Figure 7 where HR for two outbursts are plotted in different panels. In both figures, the upper and the middle panel show the variations of flux in the energy range 2–6 keV and 6–20 keV respectively as measured by MAXI/GSC. Each point on these two plots represents the one day averaged count rate. The bottom panels show the evolution of hardness (6–20 keV/2–6 keV) during the outbursts which indicate the transitions of the source through different spectral states.

The left side figure shows the variations of flux and hardness that have been plotted over 30 days (from MJD 58590 to MJD 58620) during the outburst of April when the source rose and decayed in 6–20 keV but was in the declining phase, continuing the earlier outburst of January 2019 in 2–6 keV. Initially, the source was observed to remain in the SS before initiation of the outburst, in 6–20 keV but during the outburst, the source made a transition

Table 2: Interday variation of spectral fitting parameters on different days of the outburst as observed by NuSTAR/FPMA in the energy range 3–70 keV. The spectra are well fitted with an absorbed broken powerlaw and a blackbody radiation with a Gaussian component.

Day (MJD)	n_H (10^{22} cm $^{-2}$)	τ_1	τ_2	kT_{bb} (keV)	Flux (erg cm $^{-2}$ s $^{-1}$)	χ^2_{red} (d.o.f.)
58655	0.86 (frozen)	1.2 ± 0.2	1.567 ± 0.003	0.46 ± 0.03	2.141×10^{-8}	1.259 (1665)
58660	0.86 (frozen)	1.3 ± 0.3	1.548 ± 0.003	0.51 ± 0.06	1.873×10^{-8}	1.256 (1665)
58672	0.86 (frozen)	1.0 ± 0.2	1.536 ± 0.003	0.49 ± 0.02	1.261×10^{-8}	1.267 (1665)

to HS.

In the right-side figure, the variation of flux in the energy bands 2–6 keV and 6–20 keV and their hardness have been plotted for 90 days during the June 2019 outburst using MAXI/GSC data. Variation of flux is observed in both soft and hard energy bands but photon counts in the soft band are relatively higher than that in the hard band. Throughout the outburst, the source remained in the HS with hardness ratio ~ 0.5 and the source did not show any state transition.

In the HID, the spectral state transitions of the black hole MAXI J1348–630 are shown during the outburst of April (from MJD 58596 to MJD 58614). The hardness ratio (6–20 keV/2–6 keV) is plotted using MAXI/GSC data while the flux is measured by Swift/BAT in 15–50 keV. HID for the outburst of April is shown in Figure 8. The track implies that the source made a transition from SS to HS during the outburst.

3.7. Power Density Spectra

The evolution of power spectral properties is studied during two outbursts. We have used NuSTAR and NICER data for the study of Power Density Spectra (PDS). We studied the PDS using data of all observations made by NuSTAR and NICER to investigate the possible presence of QPOs during this period. We have detected a low-frequency QPO at 0.82 Hz from NICER observation (Obs Id – 2200530160) on MJD 58654 with a bin size of 0.1 s. In Figure 9, the fitted PDS of the source using NICER observation is shown. The observation was made during the outburst of June when the source was in the HS. The PDS is well fitted with a combined model of constant, power-law and a Lorentzian. The fitted model gives the RMS value ~ 7.6 per cent and Q-value ($\nu/FWHM$) = 6.83. We have detected another QPO at 0.67 Hz using NuSTAR data (Obs Id – 80502304002) on MJD 58655 with an RMS value = 2.1 per cent and a Q-value of 5.58.

4. Discussions

In this work, we studied multi-wavelength observation of the black hole MAXI J1348–630 using ALMA, Chandra and NuSTAR during two successive outbursts of the source in April and June 2019.

During the outburst of April 2019, the source evolved through three different states. The outburst occurred when the source remained in the SS. This is because the source made a transition from HS to SS during the earlier outburst of January and it evolved through

the intermediate states and reached the HS at the end of the outburst of April. The June 2019 outburst started during the HS and the source remained in the same state throughout the outburst.

Inter-day variation of the spectral parameters was studied during the different days of the June outburst to look for the evolution of different spectral parameters. During the NuSTAR observations, the photon index and blackbody temperature did not vary significantly and the spectra were described well using the same model for different observations. This implies that probably the emission mechanism did not change significantly during this outburst.

Multi-wavelength observations are key to understand the emission properties of X-ray binaries during outbursts (viz. [Ueda et al. \(2002\)](#); [Chakrabarti et al. \(2005\)](#)). While the sources of X-ray and radio wavelength radiation is well studied, the origin of mid-energy emission in the ultraviolet, visual, and infrared is not understood properly ([Charles & Coe 2006](#)). While soft X-rays come from the inner-most regions of the accretion disk, hard X-rays could be produced by optically thin hot electron cloud due to inverse Comptonisation of the disk photons ([Done et al. 2019](#)). Radio emissions are originated from the jets due to Synchrotron emission ([Falcke & Biermann 1996, 1999](#)). We have included the radio, UV/optical and X-ray observations in the broadband spectrum. The Flux drops dramatically in the optical/UV region, probably due to the heavy extinction from the surroundings ([Paragi et al. 1999](#)).

We have detected variable PDS during two outbursts reported in the current paper. For other black holes, power spectral properties often change during an outburst ([Motta 2016](#)). In the HS and HIMS, a type-C QPO with a sharp peak is observed within a few mHz to 30 Hz. Type-B QPO is generally observed in the Soft Intermediate State (SIMS) of an outburst within the range 4–6 Hz ([Casella et al. 2004](#); [Motta et al. 2011](#); [Motta 2016](#); [Stevans & Uttley 2016](#)). Type-A QPOs are sometimes observed in the SS. They appear at frequencies similar to that of Type-B QPOs but are relatively broader ([Casella et al. 2004](#); [Motta et al. 2011](#); [Motta 2016](#); [Rodriguez et al. 2004](#); [Sriram, Rao & Choi 2013](#)). In this study, we have detected a strong QPO at 0.82 Hz from NICER observation on MJD 58654 with an RMS value of 7.6 per cent and signal to noise ratio of 6.86. The second QPO at 0.67 Hz is detected from NuSTAR observation with an RMS value of 2.1 per cent and a signal to noise ratio of 5.58. During these two detections, the source remained in the HS which is consistent with type-C QPOs typically found in black hole binaries ([Motta 2016](#); [Jana et al. 2019](#)).

We have fitted the spectra obtained from different NuSTAR observations with common models applied to study the black hole binaries. The corresponding blackbody temperature is varying between 0.46 keV and 0.51 keV which is comparatively small when the luminosity

was near to the maximum. The luminosity of the source depends on the temperature and radius of the source as $L \propto R^2 T^4$. According to the equation, a cool disk and high luminosity indicate a relatively larger disk radius. The large radius suggests that MAXI J1348–630 is massive compared to other galactic black holes.

The inner disk temperature of the disk component (kT_{in}) is related to the seed photon temperature kT_{bb} . The temperature of a standard accretion disk is inversely proportional to the black hole mass, $T \propto M^{-1/4}$ (Shakura & Sunyaev 1973). During the NuSTAR observations, the lower disk temperature of the source indicates that the system may harbor a relatively high mass black hole as stated earlier by Tominaga et al. (2020) and Jana et al. (2020).

5. Conclusion

We summarize the result of different timing and spectral evolution of the black hole X-ray binary MAXI J1348–630 during its two consecutive outbursts from MJD 58596 to MJD 58710. A study of hardness evolution shows the hardness ratio is rapidly varying during the outburst of April but remained almost constant during the outburst of June. In the HID, we found that the evolution of spectral states with intensity traces a partial ‘*q*’ shaped track but traversing in a clockwise direction. During the study of power density spectra, a QPO of 6.83σ is detected on MJD 58654 using NICER data at frequency ~ 0.82 Hz with an RMS value of 7.6 per cent. The second QPO of 5.58σ has been detected on MJD 58655 from NuSTAR data at 0.67 Hz with an RMS value of 2.1 per cent. A rapid decrease in RMS is observed. We measured the source location at RA=13h48m12.878s, Dec=−63°16'28.85" (J2000) using Chandra data. We have studied the broadband spectrum of the black hole using the flux in radio, optical, ultraviolet and X-ray energy bands during the outburst of April. The broadband spectrum suggested heavy extinction in the optical/UV region. This is probably due to the matter that has accumulated around the system. The interday variation of spectral parameters is also studied using three different observations of NuSTAR. The best fit model suggests that the disk temperature is comparatively lower than other galactic black holes which imply, the source may be relatively larger compared to most of the known galactic black holes.

Acknowledgements

In this research, we have used the necessary software like **Heasoft**, **XSPEC** etc., developed by High Energy Astrophysics Science Archive Research Center (HEASARC) at NASA-GSFC. We have also used **CIAO** and **SHERPA** developed by the Chandra X-ray Observatory team. **NUSTARDAS** tools by ESA and Caltech played important roles in this research. This research has made use of SAOImage DS9, developed by the Smithsonian Astrophysical Observatory. Data products that have been used in this research are collected from HEASARC data archives. Special thanks to Neil Gehrels Swift Observatory and MAXI-RIKEN teams since daily monitoring data of Swift/BAT and MAXI/GSC have been used in this research.

This paper makes use of the following ALMA data: ADS /JAO.ALMA#2016.1.01235.S. ALMA is a partnership of ESO (representing its member states), NSF (USA) and NINS (Japan), together with NRC (Canada), MOST and ASIAA (Taiwan), and KASI (Republic of Korea), in cooperation with the Republic of Chile. The Joint ALMA Observatory is operated by ESO, AUI/NRAO and NAOJ.

6. Data Availability

Data used in this work are available in the HEASARC browse portal provided by High Energy Astrophysics Science Archive Research Center (HEASARC) at <https://heasarc.gsfc.nasa.gov/cgi-bin>. The data that support the plots within this paper and other findings of this study are available from the corresponding author upon reasonable request. The raw ALMA data are publicly available at <https://almascience.nao.ac.jp/asax/> (project id: 2018.1.01034.T).

REFERENCES

Arnaud K. A., 1996, in Jacoby G. H., Barnes J., eds, ASP Conf. Ser. Vol. 101, Astronomical Data Analysis Software and Systems V. Astron. Soc. Pac., San Francisco, p. 17

Barthelmy S. D., et al., 2005, SSRv, 120, 143B

Belloni T. M., 2009, Lecture Notes in Physics, 794, 53

Belloni T. M., Zhang L., Kylafis N. D., Reig P., Altamirano, D., 2020, MNRAS, 496, 4366B

Belloni T., Homan J., Casella P., van der Klis M., Nespoli E., Lewin W. H. G., Miller J. M., Mendez M., 2005, A&A, 440, 207

Belloni T. M., Motta S. E., Muñoz-Darias T., 2011, *BASI*, 39, 409B

Brinkman A. C., et al., 2000, *ApJ*, 530, L111

Brown A. G. A., et al., 2018, *A&A*, 616A, 1G

Burrows D. N., et al., 2000, *SPIE*, 4140, 64B

Canizares C. R., et al., 2005, *PASP*, 117, 1144

Capitanio F., Belloni T., Del Santo M., Ubertini P., 2009, *MNRAS*, 398, 1194

Casella P., Belloni T., Homan J., Stella L., 2004, *A&A*, 426, 587

Charles P. A., Coe M. J., 2006, *csxs.book*, 39, 215

Chauhan J., et al., 2021, *MNRAS*, 501L, 60C

Chakrabarti S. K., et al., 2005, *MNRAS*, 362, 957C

Corbel S., Nowak M. A., Fender R. P., Tzioumis A. K., Markoff S., 2003, *A&A*, 400, 1007

Del Santo M., et al., 2016, *MNRAS*, 456, 3585

Denisenko D., et al., 2019, *The Astronomer's Telegram*, 12430, 1

Done C., Gierlinski M., Kubota A., 2007, *A&ARv*, 15, 1

Dunn R. J. H., et al., 2010, *MNRAS*, 403, 61

Falcke H., Biermann P. L., 1996, *A&A*, 308, 321

Falcke H., Biermann P. L., 1999, *A&A*, 342, 49

Fender R., 2006, *Jets from X-ray binaries (Compact stellar X-ray sources)*, 381, 419

Gallimore J. F., Baum S. A., O'Dea C. P., Pedlar A., Brinks E., 1999, *ApJ*, 524, 684

Gendreau K. C., et al., 2016, in *Proc. SPIE*. p. 99051H, doi:10.1117/12.2231304

Gurzadian V. G., Ozernoi L. M., 1979, *Nature*, 280, 214G

Harrison F. A., et al., 2013, *ApJ*, 770, 103

Homan J., Belloni T., 2005, *Ap&SS*, 300, 107

Homan J., Wijnands R., van der Klis M., Belloni T., van Paradijs J., Klein-Wolt M., Fender R., Mendez M., 2001, *ApJS*, 132, 377

Jana A., Debnath D., Chatterjee D., Chakrabarti S. K., Chatterjee K., Bhowmick R., 2019, *The Astronomer's Telegram*, 12505, 1

Jana A., Debnath D., Chatterjee D., Chatterjee K., Chakrabarti S. K., Naik S., Bhowmick R., Kumari N., 2020, *ApJ*, 897, 3

Kennea J. A., Negoro H., 2019, *The Astronomer's Telegram*, 12434, 1

Miller J. M., Raymond J., Reynolds C. S., Fabian A. C., Kallman T. R., Homan J., 2008, *ApJ*, 680, 1359

Motta S. E., 2016, *Astronomische Nachrichten*, 337, 398

Motta S., Muñoz-Darias T., Casella P., Belloni T., Homan J., 2011, *MNRAS*, 418, 2292

Muñoz-Darias T., Motta S., Belloni T. M., 2011, *MNRAS*, 410, 679

Negoro H., et al., 2019, *The Astronomer's Telegram*, 12838, 1

Paragi Z., Vermeulen R. C., Fejes I., Schilizzi R. T., Spencer R. E., Stirling A. M., 1999, *A&A*, 348, 910

Perley R. A., Butler B. J., 2017, *ApJ*, 230, 1538

Poole T. S., et al., 2008, *MNRAS*, 383, 627P

Remillard R. A., McClintock J. E., 2006, *ARA&A*, 44, 49

Rodriguez J., Corbel S., Kalemci E., Tomsick J. A., Tagger M., 2004, *ApJ*, 612, 1018

Sanna A., et al., 2019, *The Astronomer's Telegram*, 12447, 1

Shakura N. I., Sunyaev R. A., 1973, *A&A*, 500, 33

Sriram K., Rao A. R., Choi C. S., 2013, *ApJ*, 775, 28

Stevens A. L., Uttley P., 2016, *MNRAS*, 460, 2796

Sturner S. J., Shrader C. R., 2005, *ApJ*, 625, 923

Tominaga M., et al., 2020, *ApJ*, 899, 20

Ueda Y., et al., 2002, *ApJ*, 571, 918

van der Klis M., 2006, Rapid X-ray Variability. pp 39–112

Yatabe F., et al., 2019, The Astronomer’s Telegram, 12425, 1

Zhang L., et al., 2020, MNRAS, 499, 851Z

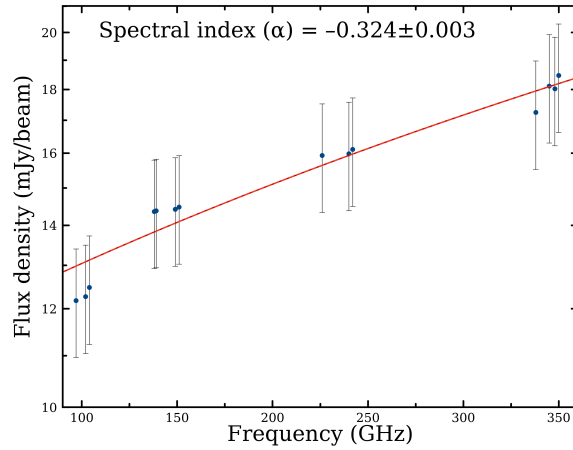


Fig. 6.— Radio continuum spectrum of MAXI J1348–630 between the frequency range of 89.56–351.44GHz with the variation of flux density between 12.18–18.47 mJy. The continuum radio spectrum shows the flat nature with spectral index (α) = -0.324 ± 0.003 (assuming $F_\nu \propto \nu^{-\alpha}$).

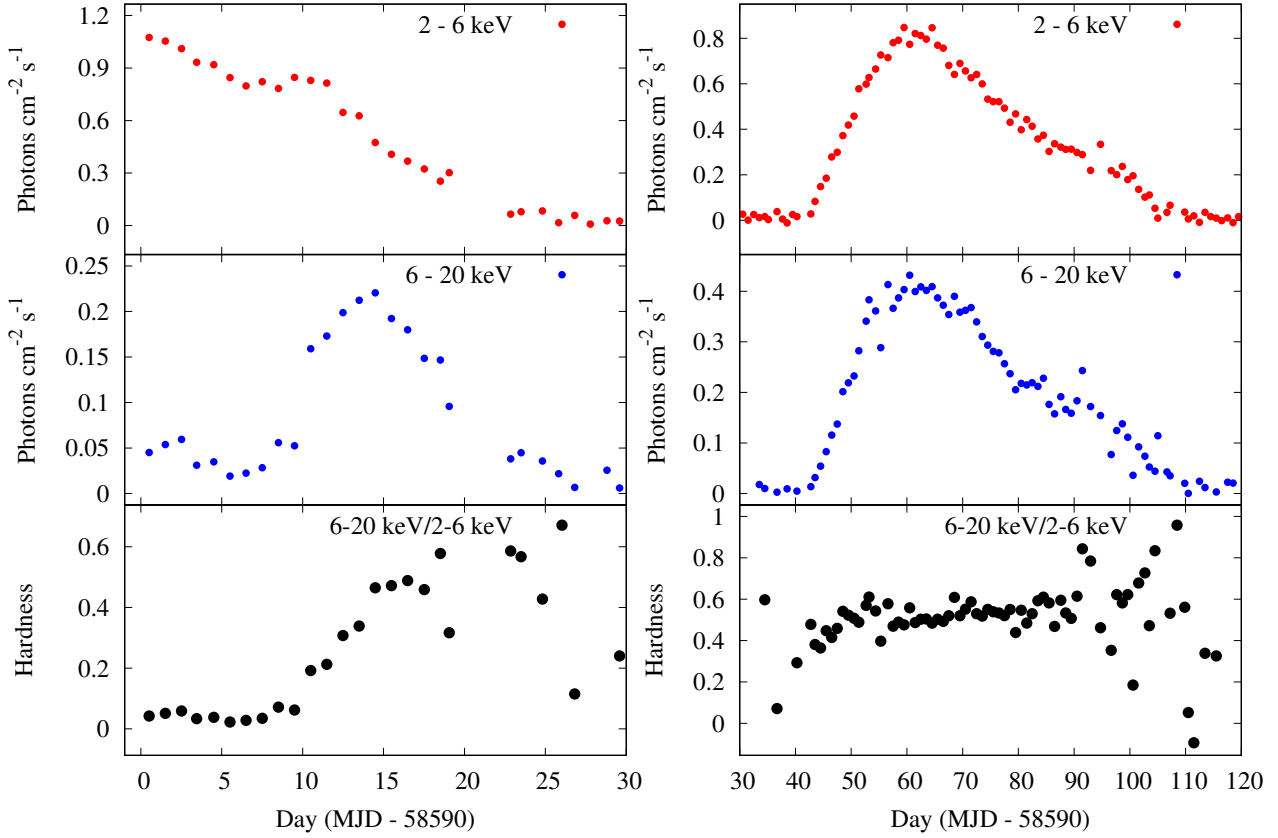


Fig. 7.— The flux of the source for two consecutive outbursts at different energy bands as well as the variation of hardness using MAXI/GSC data are plotted. In both plots, the upper and the middle panels show the variations of flux towards the source in the energy range 2–6 keV and 6–20 keV respectively. The bottom panel shows the hardness (6–20 keV/2–6 keV) of the photons during the outburst. In the left figure, the flux is negligible for soft photons whereas that for hard photons is comparatively much prominent. Variation of hardness from soft to hard is also noticeable. In the right figure, the fluxes in the different energy ranges are comparatively stronger than those in the previous one. The outburst was equally dominated by the soft and hard photons. No significant variation in hardness ratio is observed during the outburst of June 2019.

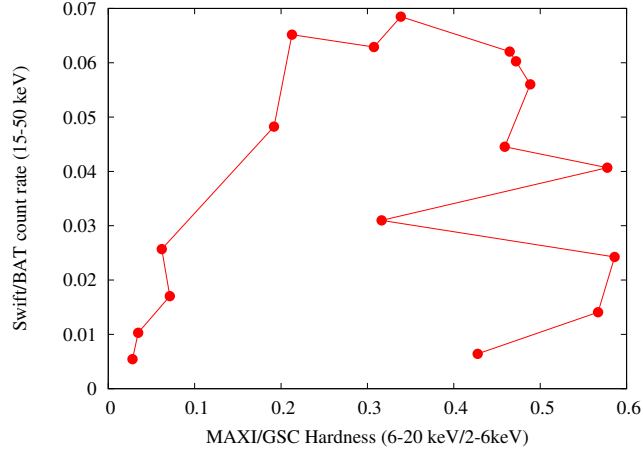


Fig. 8.— Hardness-Intensity diagram of black hole MAXI J1348–630 during the outburst of April using daily monitoring data of MAXI/GSC and Swift/BAT. The intensity has been plotted using the flux as measured by Swift/BAT in the energy range 15–50 keV and the corresponding hardness is plotted using the ratio of photon counts in 2–6 keV and 6–20 keV energy bands of MAXI/GSC. The figure shows the evolution of the source through different spectral states during the outburst.

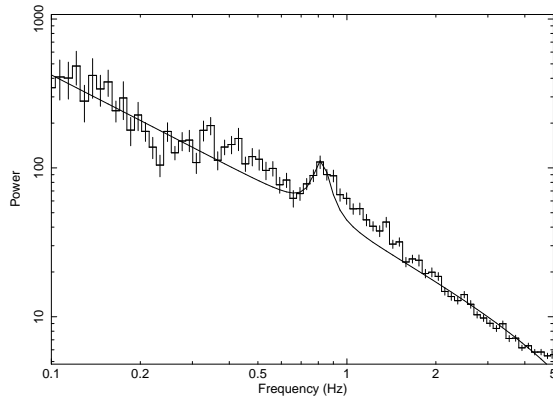


Fig. 9.— Power density spectrum of the source during the outburst of June using NICER observation with 0.1 s bin size. The presence of a low-frequency QPO at 0.82 Hz is detected with a Q-value of 6.86 and an RMS value of 7.6 per cent. The PDS is fitted with the combined model of constant, power-law and a Lorentzian component.